Acta Crystallographica Section B
Structural Science
ISSN 0108-7681

Structural phase transition to disorder low-temperature phase in $[Fe(ptz)_6](BF_4)_2$ spin-crossover compounds

Joachim Kusz,[a]* Maciej Zubko,[a] Reinhard B. Neder[b] and Phillipp Gütlich[c]

[a]Institute of Physics, University of Silesia, ul. Uniwersytecka 4, PL-40007 Katowice, Poland, [b]Lehrstuhl für Kristallographie und Strukturphysik, University of Erlangen–Nürnberg, Staudtstraße 3, D-91058 Erlangen, Germany, and [c]Institut für Anorganische Chemie und Analytische Chemie, Johannes Gutenberg–Universität Mainz, Staudinger Weg 9, D-55090 Mainz, Germany

Correspondence e-mail: kusz@us.edu.pl

Received 5 September 2011
Accepted 11 December 2011

In the spin-crossover compound $[Fe(ptz)_6](BF_4)_2$ (where ptz=1-*n*-propyltetrazole) six different phases are observed. When a single crystal is slowly cooled from high temperatures to those below 125 K, the reflections broaden into diffuse maxima and split into two maxima along the c^* direction [Kusz, Gütlich & Spiering (2004). *Top. Curr. Chem.* **234**, 129–153]. As both maxima are broad along the c^* direction, the short-range order exists only along the c direction and in the ab plane the structure remains long-range ordered. In this disordered phase additional satellite reflections appear. Upon heating above 135 K, the diffuse maxima return to their previous shape and this process is completely reversible. Rapidly cooled samples, on the other hand, do not show such splitting and the symmetry remains $R\bar{3}$, despite a jump in lattice parameters. We use a special technique to analyse the disorder model of the slowly cooled samples, which consists of layered domains shifted in the hexagonal ab plane. The low-spin disordered phase was solved in a novel approach to accommodate the very unusual twinning and refined in the non-standard space group $C\bar{1}$. In contrast to the ordered low-spin phase, the Fe ion is in a non-centrosymmetric coordination polyhedron and two of the six propyl groups change their conformation.

1. Introduction

The compound $[Fe(ptz)_6](BF_4)_2$ [hexakis(1-methylpropyl)-iron(II) bis(tetrafluoroborate)] is a fascinating spin-crossover (SCO) system. The creation of long-lived metastable spin-states by light irradiation (light-induced excited spin-state trapping, denoted as LIESST and reverse LIESST) was observed for the first time in this spin-crossover compound (Decurtins *et al.*, 1984, 1985). Numerous magnetic, optical and spectroscopic investigations have shown that $[Fe(ptz)_6](BF_4)_2$, when rapidly cooled (> 10 K min^{-1}), undergoes a thermal spin-crossover from high-spin (HS, $S = 2$) to low-spin (LS, $S = 0$) at ~ 130 K without hysteresis, but when slowly cooled (< 1 K min^{-1}) an abrupt thermal spin-crossover at ~ 125 K takes place with a hysteresis of 7 K (Franke *et al.*, 1982; Müller *et al.*, 1983; Hauser *et al.*, 1986; Ozarowski & McGarvey, 1989; Gütlich *et al.*, 1994; Jung *et al.* 1995; Jeftic *et al.*, 1996; Jeftic & Hauser, 1997; Moussa *et al.*, 2005; Goujon *et al.*, 2008; Chong, *et al.*, 2010; Zubko *et al.*, 2010). The thermal spin transition in solid transition metal compounds is characterized in a most convenient way with transition curves $\gamma_{HS}(T)$ which describe the molar ratio of molecules in the HS state as a function of temperature. The SCO phenomenon is always accompanied by a change of the metal–donor bond length and particularly a

change in the crystal lattice parameters. It is therefore possible to determine the spin state of molecules in the unit cell from diffraction measurements. These structural changes are expected to play an important role in the mechanism of the communication of a spin-state change from one complex molecule to another in the crystal lattice by cooperative interactions. A meaningful understanding of the nature of such cooperative interactions is possible only by following directly the positional changes of atoms as a function of temperature using diffraction methods especially on single crystals (Gütlich & Goodwin, 2004).

The spin-crossover complex $[Fe(ptz)_6](BF_4)_2$ is very interesting from a crystallographic point of view. The complex has only one type of lattice site for the iron(II) centres, but it is possible to generate six different phases depending on the rate of cooling of the sample on the one hand and by irradiation with light on the other.

The compound $[Fe(ptz)_6](BF_4)_2$ was first synthesized and characterized as a thermal SCO system by Franke *et al.* (1982). It crystallizes in the rhombohedral space group $R\bar{3}$. The six different phases observed in this compound are discussed in the following.

(i) In the high-temperature phase (denoted as *HS-R3*) the molecules are in the stable HS state down to the spin transition temperature $T_{1/2}$ = 130 K and the crystal possesses the high symmetry ($R\bar{3}$) structure. Structures of this phase were investigated using single-crystal X-ray diffraction (Franke, 1982; Wiehl, 1993; Kusz, Spiering & Gütlich, 2004) and also with synchrotron powder diffraction and Rietveld analysis (Moritomo *et al.*, 2002*a*). The high-spin Fe^{II} ion is in a special position 3*a*: 0,0,0 (site symmetry $\bar{3}$) and all three $[Fe(ptz)_6]^{2+}$ complexes are symmetrically equivalent through the *R* centring translations. All ligands are equivalent according to the $\bar{3}$ symmetry. The anions lie on the threefold axis, where the B and F atoms occupy the positions 6*c*: 0,0,*z* and 0,0,−*z* (site symmetry 3). The cationic $[Fe(ptz)_6]^{2+}$ complexes and the $(BF_4)^-$ anions form layers perpendicular to the *c* axis and the order within the layers is exactly trigonal. Adjacent layers are shifted parallel to the planes according to the rhombohedral stacking. The stacking period is triple. The distance between layers is *ca* 11 Å. The bond distances for the FeN_6 core are nearly independent of temperature and for the HS state ($T > T_{1/2}$) they are 2.20 Å.

(ii) After cooling below the spin transition temperature (135 K), it is possible to observe two different kinds of LS phases: a LS supercooled-ordered phase (denoted *LS-ord*) and a disordered LS phase (denoted *LS-dis*). Ozarowski & McGarvey (1989) first observed in an EPR study on a single crystal of this compound doped with Mn^{II} and Cu^{II} that two different LS phases may be generated depending on the rate of cooling the sample through the spin transition region. When the crystal is cooled quickly from 135 to 90 K, the spin transition is abrupt and without hysteresis at $T_{1/2}$ = 130 K. This LS supercooled phase exists only below 100 K. The structure of this second phase was investigated by synchrotron powder diffraction and Rietveld analysis (Moritomo *et al.*, 2002*a*), and the X-ray single-crystal method (Kusz, Spiering & Gütlich, 2004). The LS supercooled phase (*LS-ord*) is very similar to the high-temperature phase and also belongs to the rhombohedral space group $R\bar{3}$ (Z = 3), because the structure of the HS high-temperature phase is quenched by rapid cooling (Moritomo *et al.*, 2002*a*; Kusz, Spiering & Gütlich, 2004). The bond distances of the LS FeN_6 core are also nearly independent of temperature but decrease by *ca* 10% to 2.00 Å upon spin transition. The *a* axis decreases with spin transition from 10.89 to 10.74 Å, while the *c* axis increases from 31.94 to 32.14 Å (Kusz *et al.*, 2000; Kusz, Gütlich & Spiering, 2004). These observations clearly demonstrate that when the crystal is rapidly cooled, the spin transition is not triggered by a structural phase change, *i.e.* the spin transition takes place independently of the crystallographic change.

(iii) The third phase is the metastable HS phase which exists below 50 K after rapid cooling and after irradiation with green light (514 nm) of an Ar laser. This phase will be denoted as the *LIESST-HS-ord* phase. Many iron(II) complexes exhibiting thermal spin-crossover may be converted from the $^1A_1$ diamagnetic low-spin (LS) state to the $^5T_2$ paramagnetic high-spin (HS) state by irradiation with green light (514 nm) (Gütlich *et al.*, 1994). The lifetime of the metastable LIESST state is often sufficiently long for X-ray diffraction studies. The first structure of a photoexcited state created by LIESST and reverse-LIESST was carried out with the $[Fe(mtz)_6](BF_4)_2$ spin-crossover compound (Kusz, Spiering & Gütlich, 2001). The structure of the LIESST phase of $[Fe(ptz)_6](BF_4)_2$ was investigated on a single crystal with polarized neutron diffraction (Jeftic *et al.*, 2003; Goujon *et al.*, 2006) and X-ray diffraction (Kusz, Spiering & Gütlich, 2004). A single-crystal structure for $[Fe(ptz)_6](BF_4)_2$ on the supercooled (*LS-ord*) phase and the *LIESST-HS-ord* phase was refined at 10 K. At this low temperature the light-induced spin-state conversion was complete and the lifetime of the metastable LIESST state was practically infinitely long. The structure of the HS supercooled phase after LIESST (*LIESST-HS-ord*) is very similar to that of the high-temperature phase and belongs to the same rhombohedral space group $R\bar{3}$ (Z = 3). The following metal–donor atom distances, d(Fe—N), have been found at 10 K: 2.18 Å in the HS (LIESST) state and 1.99 Å in the LS state (Kusz, Spiering & Gütlich, 2004). The d(Fe—N) values determined at 80 K at the supercooled LS phase are 1.99 and 2.17 Å at 160 K in the HS state (Kusz, Spiering & Gütlich, 2004).

(iv) The other possible HS phase described by Moritomo *et al.* is a photo-induced metastable phase which can exist above 50 K (denoted as the *HS-exc-ord* phase). Above a critical light intensity the photo-excited HS molecules in metastable domains develop and this can be interpreted in terms of the condensation of the photo-excited $[Fe(ptz)_6]^{2+}$ units. Moritomo *et al.* (2002*b*) observed this novel phase at 91 K on a powder sample irradiated with synchrotron radiation when the excitation power with green laser light exceeded the critical value (55 mW). The photo-induced change of the X-ray powder pattern disappeared quickly to restore the pre-excitation pattern when the photo-excitation was stopped. This means that the structural changes are maintained only

under continuous photo-excitation. The change in the powder pattern is completed in less than 1 min at 91 K. This phase is also rhombohedral with the space group $R\bar{3}$. The Fe—N bond distance determined by Rietveld structural analysis is 2.1 Å and the lattice parameter a = 10.82 Å. Both values are much smaller than the corresponding value for the high-temperature structures, but above the critical power it changes from the LS to the HS values proportional to excitation power (Moritomo *et al.*, 2002*b*).

This phase, however, is in sharp contrast to the so-called *LIESST-HS-ord* phase in which the photo-excitation induces a structural change into a metastable one and the structure is permanently maintained after turning off the laser.

(v) Crystal structure of $[Fe(ptz)_6](BF_4)_2$ after slow cooling (disordered LS phase). During slow cooling and heating ($\Delta T < 1$ K min^{-1}), $[Fe(ptz)_6](BF_4)_2$ also shows an abrupt and complete spin transition but with hysteresis ($T_{1/2}\downarrow \simeq 128$ K, $T_{1/2}\uparrow \simeq 135$ K; Gütlich *et al.*, 1994). Single-crystal X-ray measurements showed that the low-spin, low-temperature crystallographic phase (denoted *LS-dis* phase) gives diffuse reflections and therefore is named as disordered (Kusz *et al.*, 1996; Kusz, Gütlich & Spiering, 2004; Lakhloufi *et al.*, 2010). From the initial X-ray powder diffraction measurements it was proposed that the spin transition is accompanied by a first-order structural phase transition (Wiehl *et al.*, 1990).

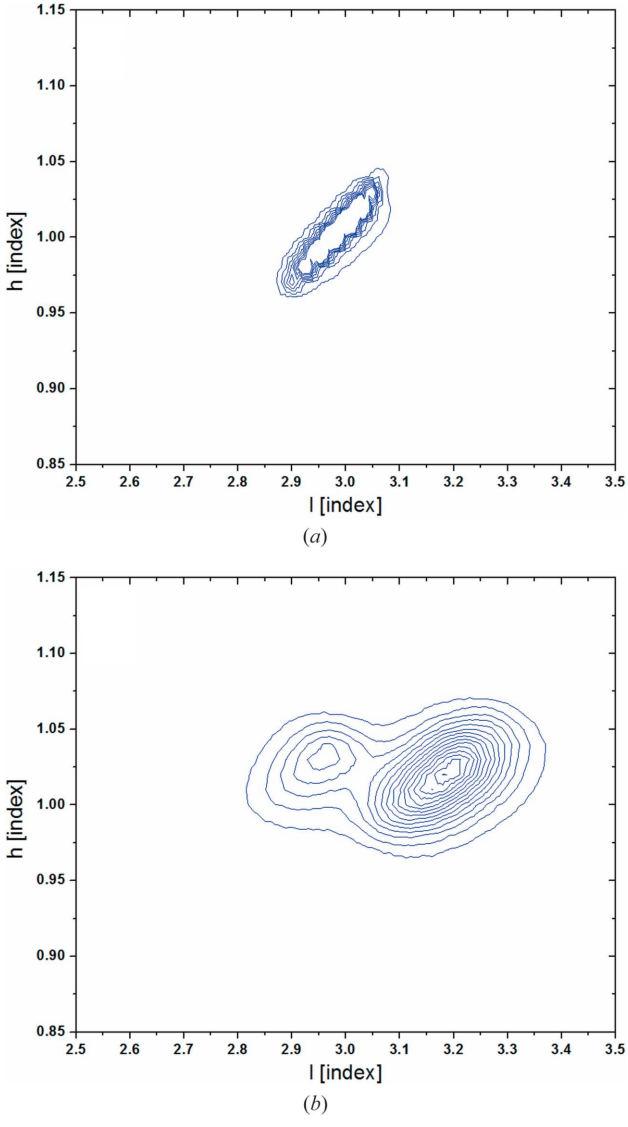

Figure 1
Two-dimensional *hl* q-scan of the 113 Bragg peak at (*a*) 140 K (*HS-R3* phase) and (*b*) 70 K (*LS-dis* phase). The elongated reflection shape in the *HS–R3* phase is associated with the experimental setup.

The structure of the LS disorder phase formed by slow cooling (*LS-dis* phase) is substantially different from the structure of the HS phase (*HS-R3*). When the sample is rapidly cooled to below $T_{1/2}$ = 135 K, significant changes of the lattice parameters are observed upon the transition to the LS state, but the Bragg reflections remain sharp (Kusz *et al.*, 2000). However, when the sample is cooled slowly from high temperatures to temperatures below 135 K, the lattice parameters change simultaneously with the spin transition and then the reflections broaden slowly and split into two maxima along the c^* direction (Fig. 1). The time needed for this crystallographic phase transition to be completed is *ca* 30 min and depends on temperature and crystal quality.

Franke (1982) previously noted that the $[Fe(ptz)_6](BF_4)_2$ crystal at 100 K was no longer a 'single crystal in the crystallographic sense'. The broadening and splitting of the peaks in the single-crystal X-ray diffraction pattern were previously interpreted on the basis of powder data as only resulting from a structural phase transition from the rhombohedral space group ($R\bar{3}$) to the triclinic space group $P\bar{1}$ (Wiehl *et al.*, 1990). From conventional X-ray powder measurements and without Rietveld refinement it is difficult to decide whether the low-temperature phase is ordered or disordered. Moritomo *et al.* (2002*a*) first confirmed from synchrotron radiation experiments and using the Rietveld method that the X-ray powder pattern of $[Fe(ptz)_6](BF_4)_2$ becomes 'disordered' if the sample is held at temperatures adjacent to the spin-crossover temperature longer than 5 min. Recently Lakhloufi *et al.* (2010) refined the structure of the disordered phase as superstructure $2ax2bxc$ in the space group $R\bar{3}$ with R = 0.19, but for this superstructure it is not clear why satellite reflections are not split in contrast to the Bragg reflections.

The structural properties of the low-spin phase formed at low temperature after slow cooling (*LS-dis* phase) have never been clearly elucidated. In this paper we discuss our hitherto existing results. We also describe the sixth HS disordered phase which exists below 50 K after slow cooling and irradiation with green laser light (denoted *LIESST-HS-dis* phase)

2. Experimental

A sample of $[Fe(ptz)_6](BF_4)_2$ was prepared as described by Franke *et al.* (1982). Single crystals were obtained after recrystallization of $[Fe(ptz)_6](BF_4)_2$ from nitromethane. The compound crystallizes as colorless hexagonal plates which are optically unaxial. The crystals are mechanically very soft but sufficiently stable for diffraction studies. Good quality single crystals of approximate dimensions *ca* 0.5 × 0.5 × 0.2 mm

were selected with a polarization microscope and examined by X-ray Mo radiation with the Laue method. Control measurements showed that the space group is $R\bar{3}$.

For the first measurement of diffuse scattering in $[Fe(ptz)_6](BF_4)_2$ the classical film methods have been applied, *e.g.* the Weissenberg or precession method (Wiehl, 1993; Kusz, Böhm & Gütlich, 2001). These methods do not provide reliable intensities for the analysis of reciprocal space and performing computer simulations of diffuse scattering. The use of diffractometers is more appropriate. In order to obtain an X-ray flux of high intensity our four-circle Huber diffractometer was combined with a Cu $K\alpha$ Enraf–Nonius rotating anode and controlled with a PC computer using the Stoe STADI4 program system (Stoe, 1995). This diffractometer was equipped with a two-stage closed-cycle helium low-temperature attachment (CTI-Cryogenics) with a Be cap. The single crystals were mounted with soft adhesive vacuum grease on a copper needle on the cold head of the second stage. For LIESST effect studies we irradiated the crystal in the LS disordered phase at 10 K using an Ar+ laser (λ = 514.5 nm) from Coherent Innova Ar with fibre optics (Kusz *et al.*, 2000). The intensities of Bragg reflection profiles were scanned along the directions of a^*, b^* and c^* (q-scan) at different temperatures.

For the determination of the disordered structure, the data were collected on an Xcalibur four-circle diffractometer with a Sapphire3 CCD detector and Mo $K\alpha$ radiation (λ = 0.71073 Å) with a graphite monochromator. Data reduction and reconstruction of reciprocal space were performed using the *CrysAlis* (Agilent, 2010) program. To properly integrate split reflections for the disordered structure (*LS-dis*) the profile learning method was used and additionally the resulting integrating mask was increased to 1.25 its original size. During data reduction, further control of the integration

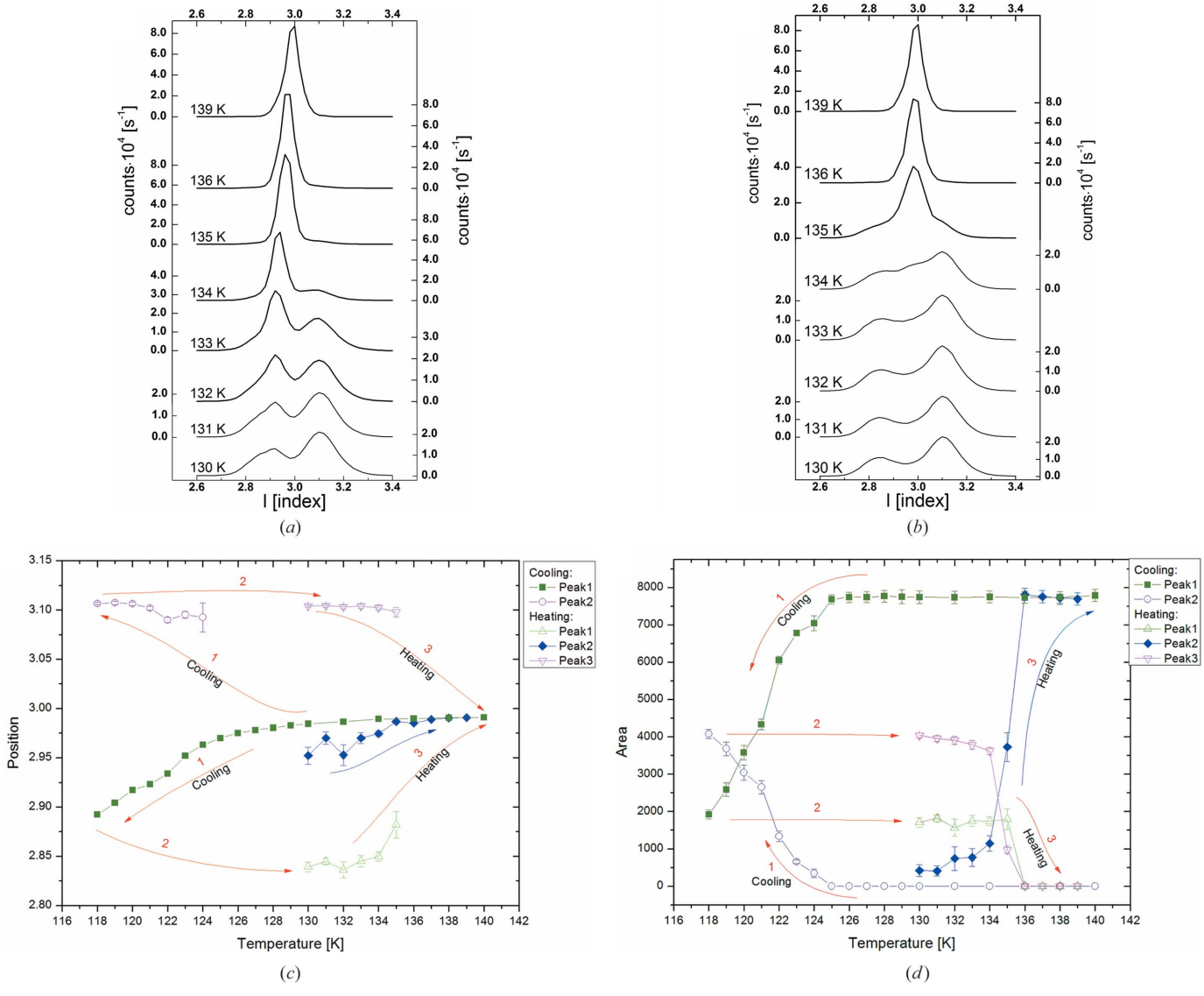

Figure 2
A sequence of q-scans of the 113 Bragg reflection during (*a*) slow cooling from 140 K (*HS-R3* phase) to 118 K (*LS-dis* phase) and (*b*) subsequent heating to 139 K (*HS-R3* phase). The corresponding changes of (*c*) peak positions and (*d*) peak intensities.

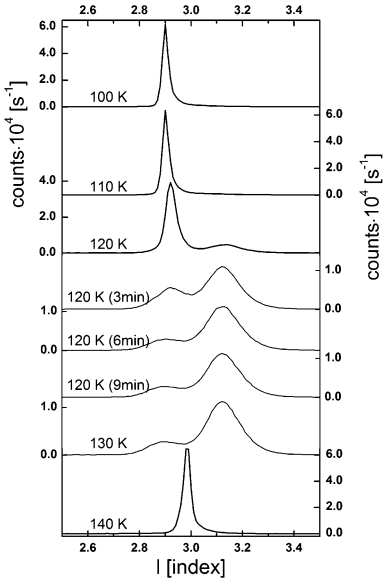

Figure 3
Sequence of q-scans of the 113 Bragg reflection. The sample was quickly cooled to 100 K, then slowly heated up to 120 K. At 120 K the temperature was kept constant for 10 min, followed by slow heating to 140 K (*HS-R3* phase).

process was carried out. A crystal of dimensions 0.14 × 0.53 × 0.61 mm^3 was mounted with vacuum grease on a quartz glass capillary and cooled by a cold dry nitrogen gas stream (Oxford Cryosystems equipment). The temperature stability was ±0.1 K. Data were collected at 84 K for the *LS-ord* phase after rapid cooling (10 K min^{-1}) and for the *LS-dis* phase after slow cooling (1 K min^{-1}) from 140 K.[1]

3. Results

In order to accurately analyse the phase transition from the ordered HT phase (*HS-R3*) to the disordered LT phase (*LS-dis*) initial measurements were performed on a four-circle diffractometer with point detector in reciprocal space directions a^*, b^* or c^* (q-scans) for selected Bragg reflections.

The two-dimensional q-scan (Fig. 1) of the 113 Bragg reflection at 140 K (*HS-R3* phase) and at 70 K (*LS-dis* phase) shows that diffuse scattering develops along the c^* direction during cooling. A thorough analysis of the measurement presented in Fig. 1 shows that the ratio of the width of the reflexes in the direction of c^* to the width in the direction of a^* before the phase transition (*i.e.* at 140 K) is equal to 3.12 and after the phase transition (at 70 K) is 8.82. These results indicate that correlations in crystal structure along the c axis are of short-range nature, whereas those along the a and b axes are of long-range nature.

To speed up the peak-profile investigations, the measurements were limited to one-dimensional q-scans in the c^* direction. Fig. 2 shows the changes of the 113 peak profile during cooling from 140 (*HS-R3* phase) to 118 K (*LS-dis* phase) (Fig. 2*a*) and subsequent heating to 139 K (*HS-R3* phase) (Fig. 2*b*). While slowly cooling, the Bragg peak splits into two maxima and during heating a third maximum develops in between the split peaks indicating the reappear-

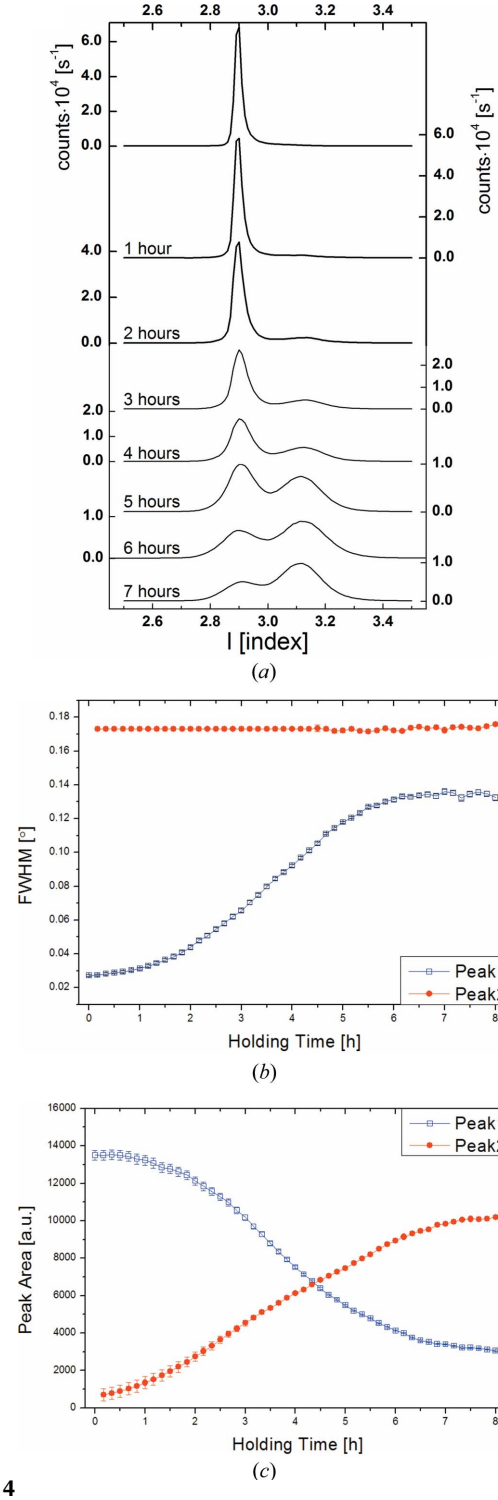

Figure 4
A time-dependent sequence of (*a*) q-scans of the 113 Bragg reflection at constant temperature after quick cooling to 100 K. This figure shows the slow structural phase transition from the LS supercooled phase (*LS-ord*) to the LS disordered phase (*LS-dis*). Time dependence of (*b*) FWHM and (*c*) peak intensity. Fig. 4(*a*) shows selected q-scans from the full time series shown in (*b*) and (*c*).

[1] Supplementary data for this paper are available from the IUCr electronic archives (Reference: PC5004). Services for accessing these data are described at the back of the journal.

ance of the HT phase. In the HS state the peak profile returns to the original shape (Fig. 2*b*). Figs. 2(*c*) and (*d*) show changes of position and intensity of the 113 peak during the phase transition.

This cycle was repeated with the same sample and the transition (both the structural and the spin transition) is fully reversible. This proves that the profile change of the Bragg peak is not associated with breaking of the single crystal.

The disordered LS phase (*LS-dis*) can be obtained not only from the HS phase (*HS-R3*) during slow cooling but also from the LS supercooled phase (*LS-ord*) during slow heating (Fig. 3). Measurements showed that at 120 K the conversion to the LS disordered phase (*LS-dis*) takes place and upon further heating at 140 K the sample returns to the HS state which is accompanied by a structural phase transition to the high-temperature phase (*HS-R3*).

It is also possible to convert the LS ordered phase (*LS-ord*) to the low-spin disordered phase (*LS-dis*) by holding the sample at temperatures close to the spin-crossover (100–135 K) for a sufficiently long time. Fig. 4(*a*) shows the time-dependent conversion of the LS ordered phase (*LS-ord*) to the LS disordered phase (*LS-dis*) at 100 K.

During the very slow structural phase transition at 100 K a weak second peak appears whose position slightly shifts during the transition. Its FWHM remains constant, while the FWHM of the main peak, which corresponds to the ordered phase, clearly increases with increasing time (Fig. 4*b*). It is important to stress that the integral intensity of both peaks does not change while the second maximum arises at the cost of the first maximum (Fig. 4*c*).

The dynamics of this conversion strongly depend on temperature. At 100 K the structural phase transition takes place over *ca* 7 h (Fig. 4). Similar measurements performed at 90 K showed that after 2 d no significant change of the peak profile had been noticed while at 120 K the structural phase transition takes place within *ca* 10 min (see Fig. 3).

In order to find out whether a disordered phase can occur in the metastable HS state and whether there are any differences between these two phases, single crystals in the LS diffuse phase (*LS-dis*) were irradiated with green laser light at 10 K. As shown in Fig. 5(*a*), the irradiation did not lead to ordering of the diffuse phase structure (*LIESST-HS-dis*) but the diffuse peaks were only shifted to the direction of lower *l* values with irradiation time. In this HS diffuse phase (*LIESST-HS-dis*) the distance along *c** between the two maxima and their FWHM increases with time (Fig. 5*b*). After heating the crystals up to 50 K, the sample returns to the LS disordered phase (*LS-dis*) and the distance between the two split maxima and their FWHM again decreases (Fig. 5*b*). This means that this process is reversible and it is not associated with a crystallographic phase transition. During light irradiation, the transition to the HS phase occurred after approximately 40 min; this is longer

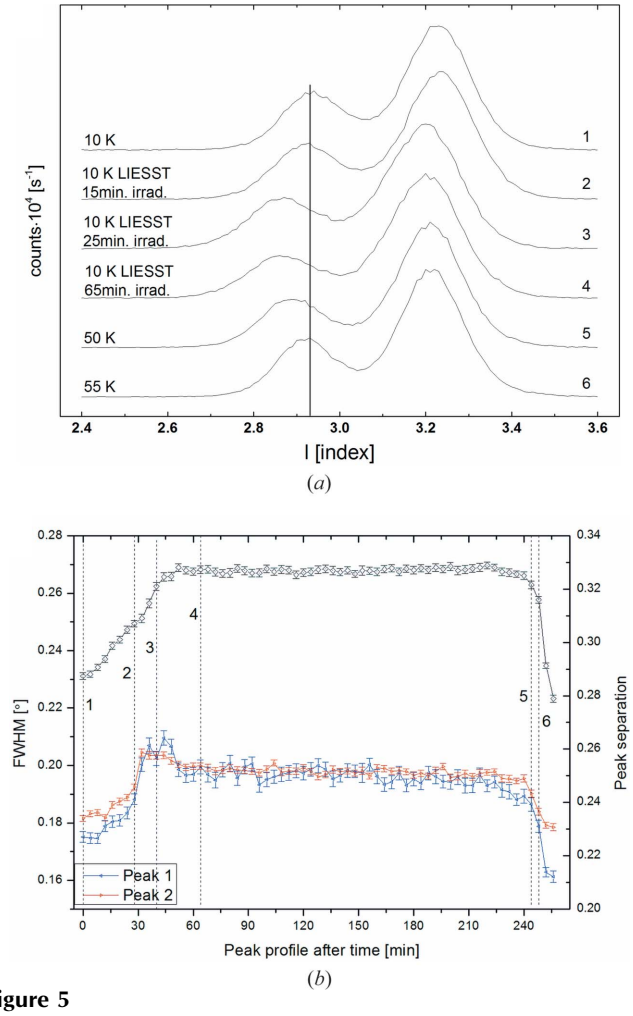

Figure 5
Change of 113 peak profile during the LIESST process of the *LS-dis* phase. (*a*) Selected *q*-scans after different irradiation times and temperature. (*b*) FWHM and peak separation as a function of the LIESST process. At t = 0 the irradiation was switched on and kept constant for 65 min (vertical line 4, *q*-scan 4). From t = 65 to t = 245 min the sample temperature remained constant and was then heated to 55 K where the spin transition to the LS state occurred.

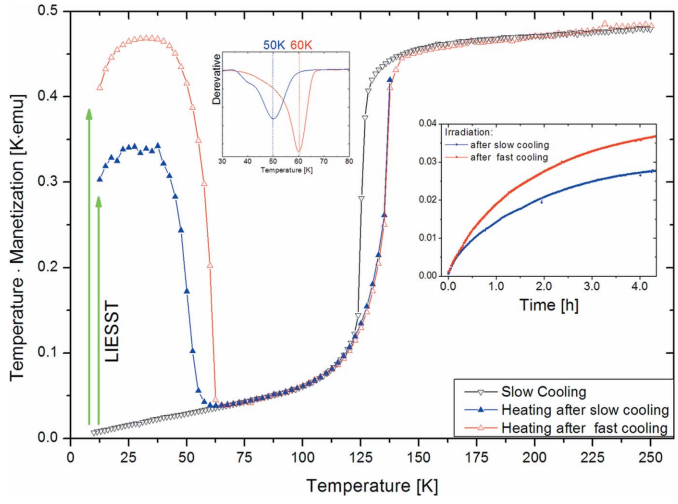

Figure 6
SQUID magnetic measurement of the $[Fe(ptz)_6](BF_4)_2$ compound by fast (red) and slow (blue) cooling rate and LIESST phenomena (green). Insets show the derivative of the relaxation curves after LIESST indicating the phase transition temperatures and the time dependence of 'temperature···magnetization' during light irradiation at 10 K.

in comparison to the ordered phase (Kusz *et al.*, 2000). During the transition from the *LS-dis* to the *LIESST-HS-dis* phase a significant increase of FWHM for both peaks of the 113 Bragg reflection is observed. This points at an increase of structural disorder of the high-spin phase in comparison to the low-spin phase. In order to compare structurally the HS disordered phase after LIESST (*LIESST-HS-dis*) with the HS ordered phase after LIESST (*LIESST-HS-ord*), magnetic measurements on a SQUID magnetometer were performed (Fig. 6). A thin single crystal of $[Fe(ptz)_6](BF_4)_2$ was quickly cooled down to 10 K and irradiated at that temperature in the LS supercooled phase (*LS-ord*) with green laser light for 240 min. Afterwards, the sample was heated up to 250 K (Fig. 6). During heating the sample was irradiated up to 100 K. The whole procedure was repeated with slow cooling in order to obtain the LS disordered (*LS-dis*) phase. As shown in Fig. 6, in the (*LIESST-HS-dis*) disordered phase cooperative interactions appear to be weaker due to the fact that in spite of the same irradiation conditions (240 min and the same laser power) a smaller number of molecules were converted into the HS state. This phenomenon was also observed in NIS (nuclear inelastic scattering of synchrotron radiation) measurements (Böttger *et al.*, 2006). Beside this the temperature of fastest decay of the metstable HS state after LIESST $-$ $T(LIESST)_{dis}$ = 50 K is for the disordered phase (*LIESST-HS-dis*) significantly lower than for the ordered phase (*LIESST-HS-ord*) $T(LIESST)_{ord}$ = 60 K, of course for comparable decay times.

3.1. Computer simulations of the time evolution of the disordered phase (*LS-dis*)

In order to understand the disordered phase and the dynamics of the structural phase transition, computer simulations of diffraction peak profiles have been performed. Simulations and refinement of peak profiles have been performed with the *DISCUS* program package (Proffen & Neder, 1997; Neder & Proffen, 2008).

As the splitting of Bragg peaks occurs along the *l* direction, the simplest and the most straightforward model could assume the creation of two types of domains with a different *c* lattice parameter, *i.e.* different interlayer distances. This model can, however, be excluded as the observed 00*l* reflections do not split.

The simplest successful model is based on stacks of identical perfect trigonal layers which are stacked either by the rhombohedral centring vector $[\frac{1}{3}, -\frac{1}{3}, \frac{1}{3}]$ (*R*) or by the rhombohedral centring vector with an additional shift δ of $[\frac{1}{3} + \delta_x, -\frac{1}{3} + \delta_y, \frac{1}{3}]$ (*R*′). In this model 00*l* reflections are not split and the splitting distance of other reflections increases with an increasing *h* or *k* index. Such a microdomain model has been chosen on the basis of lattice parameter changes observed during the spin transition. The *c* parameter rapidly increases during the spin transition expanding the molecular layers and weakening the interaction forces which stabilizes the structure.

The applied model is characterized by three parameters describing: the additional shift between adjacent layers

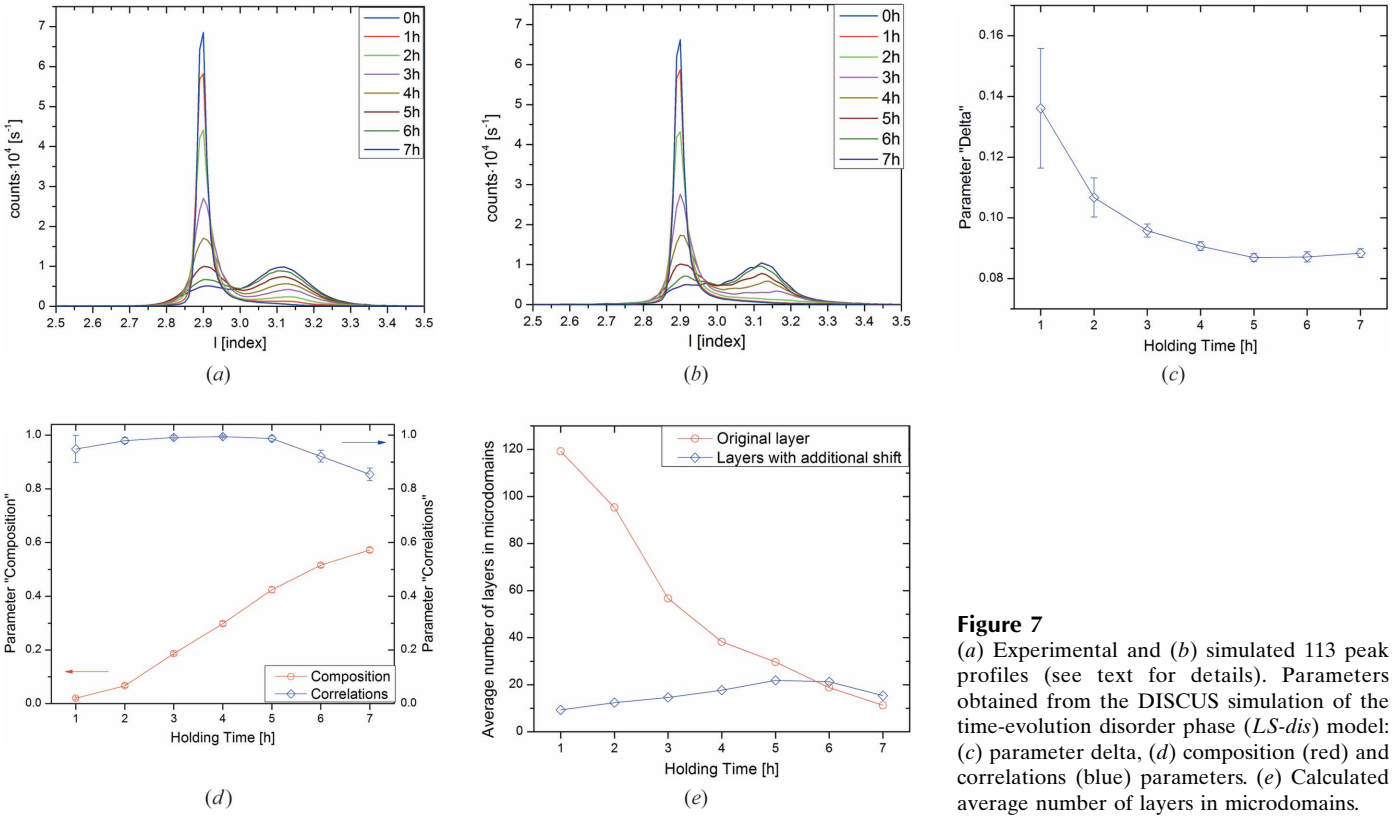

Figure 7
(*a*) Experimental and (*b*) simulated 113 peak profiles (see text for details). Parameters obtained from the DISCUS simulation of the time-evolution disorder phase (*LS-dis*) model: (*c*) parameter delta, (*d*) composition (red) and correlations (blue) parameters. (*e*) Calculated average number of layers in microdomains.

(*parameter delta*), the percentage of additionally shifted layers (*composition parameter*) and the correlations along the *c* direction between shifted layers (*correlation parameter*). The parameters have physical meaning for ($0 \leq$ *composition* ≤ 1) and ($-1 \leq$ *correlation* ≤ 1).

When the *delta* parameter is increased, layers of the second type are shifted by a larger distance, which increases the distance between two peak maxima. In turn, a larger composition parameter, which amounts to a larger number of shifted layers, increases the intensity ratio between split peaks. Finally, the correlation parameter influences the stacking patterns by aggregating layers of the same type, *i.e.* creates larger domains, which influences the width of simulated peaks.

There were 40 sets of parameters which were optimized using a differential evolutionary algorithm (Proffen & Neder, 1997; Neder & Proffen, 2008) implemented in the *DISCUS* software package. The difference between the intensity of measured and calculated peak profiles was used as the minimized function (quality of the fit).

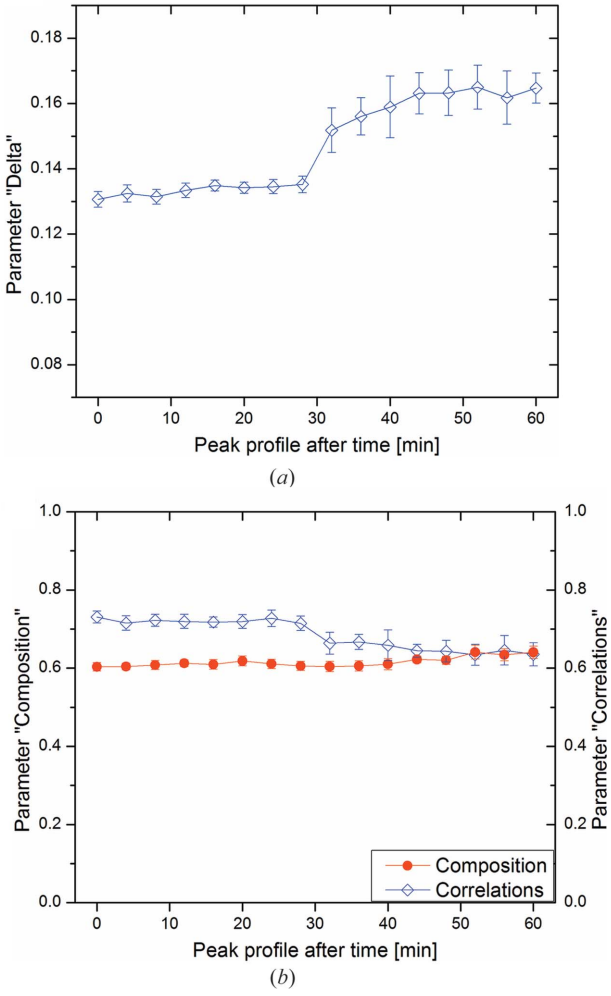

Figure 8
Parameters obtained from the DISCUS simulation of the LIESST evolution disorder phase (*LIESST-HS-dis*) model: (*a*) parameter delta; (*b*) composition (red) and correlations (blue) parameters. This figure is in colour in the electronic version of this paper.

Each of the simulated crystals [size $1a \times 1b \times (500/3)c$] consisted of 500 layers perpendicular to the *c* axis. At the beginning a random set of microdomains of the second type was selected on the basis of the *composition* parameter. In the next step in 200 000 cycles, the layers were randomly exchanged in order to satisfy the *correlation* parameter. In the last step, the layers of the first type were created according to the vector *R* and of the second type according to the vector *R*′ (depending on the *delta* parameter). Layers of both types were derived from the solution of an ordered phase and treated as rigid bodies.

For each set of parameters – 30 crystal models were generated, in order to obtain the statistically averaged intensity of the studied peak profile, which was compared with the measured reflection. On this basis, using a differential evolutionary algorithm, 40 new sets of parameters were determined.

Due to the experimental setup (rectangular slits in front of the point detector) the obtained peaks, even in the *HT-R3* phase, possess asymmetry (see Figs. 1 or 3). In order to compare the simulation with the experiment, we had to convolute results obtained from the simulations with a shape function. The shape function was determined on the basis of Bragg peaks in the ordered phase (*HS-R3*) using the basic learnt profile method (Gałdecka, 2002). The refinement of the proposed model converged and calculated peak profiles are in good agreement (see Fig. 7*b*) with experimental peak profiles (see Fig. 7*a*). Figs. 7(*c*) and (*d*) show the development of the model parameters as a function of holding time during the constant temperature experiment reported in Fig. 4. The additional shift between layers (*delta*) initially decreases. After 3 h it remains essentially constant with time at a value of $0.1a$ which approximately corresponds to an additional shift of 1 Å. The large standard deviation for the data obtained after a 1 or 2 h holding time arises from the fact that the second peak is poorly resolved and its position is difficult to locate. The value of the '*composition*' parameter increases constantly with holding time. This indicates that the number of molecular layers that belong to a microdomain of the second type increases constantly with holding time.

For the first 5 h of holding time, the parameter '*correlations*' yielded values very close to 1.0, which indicates that the same type of layers assemble next to each other. After 5 h holding time, once the '*composition*' parameter increases beyond 0.4 the parameter '*correlations*' began to decrease. Such behaviour points to the existence of a preferred microdomain size. From obtained parameters, it is possible to determine the average microdomain thickness by generating a statistically sufficiently large number of structures and calculating the average microdomain size (Fig. 7*e*). The refinements show that with increasing holding time, more and more new microdomains form. The size of the original domain thereby decreases. The obtained sizes for both microdomain types remain similar for holding times longer than 6 h. This result is also in agreement with the observed increase of the FWHM of studied *q*-scan peak profiles (Fig. 4*c*). The computer simulations thus give insight into the real structure of the disordered

phase of the $[Fe(ptz)_6](BF_4)_2$ compound pointing at the formation of lamellar microdomains perpendicular to the *c* direction. Optical measurements confirmed the creation of microdomains (Chong *et al.*, 2010).

3.2. Computer simulations of the evolution of the disordered (*LS-dis*) → (*HS-LIEST-dis*) phase after LIESST

Changes of the 113 peak profile during irradiation of the disordered LS phase (*LS-dis*) with green laser light are

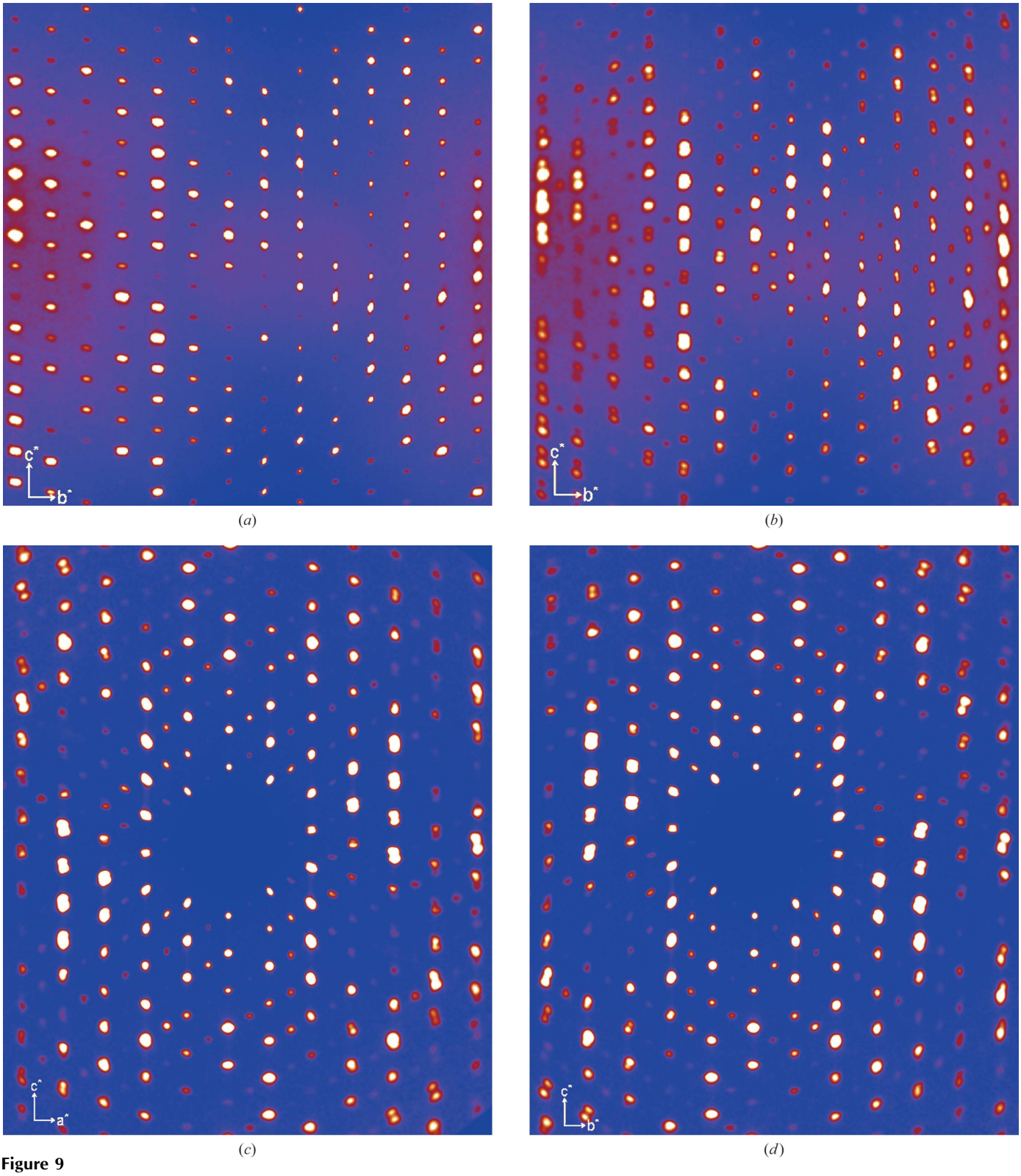

Figure 9
Hexagonal (3*kl*) layer at 84 K for (*a*) the LS supercooled phase (*LS-ord*) and (*b*) the LS disordered phase (*LS-dis*). Hexagonal (*c*) (*h*0*l*) layer and (*d*) (0*kl*) layer at 84 K in the LS disordered phase (*LS-dis*).

presented in Fig. 5(*a*). Using the model described above, computer simulations were performed in order to obtain information on the structural differences in the disordered LS phase (*LS-dis*) and the disordered HS phase (*LIESST-HS-dis*). Calculations performed for succeeding peak profiles showed that during light irradiation of the disordered LS phase, the parameter *delta* significantly increases (Fig. 8*a*) implying an increase of the shift between adjacent layers in the HS state in comparison to the LS state. The parameter *correlation* slightly decreases and the parameter *composition* remains constant (Fig. 8*b*)

During the transition to the *LIESST-HS-dis* phase structural disorder increases. This is seen in the decrease of the correlation parameter (Fig. 8*b*) and also in the increase of the FWHM peak (see Fig. 5*b*). The number of layers that belong to the second type is consistent. The above-mentioned studies show that both disordered phases – low-spin (*LS-dis*) and high-spin (*LIESST-HS-dis*) – are created by microdomains. The results obtained from the simulations are consistent with hitherto existing results and suggest that in $[Fe(ptz)_6](BF_4)_2$ the structural phase transition to the disordered *LS-dis* phase is connected with the slow process of creating micro twins. As such a phase transition is not observed in the isostructural complex $[Zn(ptz)_6](BF_4)_2$ (Kusz *et al.*, 2000), it may suggest that a significant increase of the distance between adjacent electrically neutral layers originated during the spin transition (from 10.647 to 10.713, *i.e.* 0.066 Å; Kusz, Spiering & Gütlich, 2004) weakens the van der Waals forces between layers and is responsible for this structural phase transition. It is interesting that this structural phase transition takes place only in the temperature range 100–135 K and its dynamics strongly depend on temperature. For the diluted compounds $[Fe_xZn_{1-x}(ptz)_6](BF_4)_2$, where $x < 0.5$, the phase transition to the *LS-dis* phase vanishes owing to the fact that the changes in interlayer distances are too small (from 10.637 to 10.644 this is 0.007 Å; Kusz, Spiering & Gütlich, 2004).

3.3. X-ray analysis of the phase transition to the disordered structure (*LS-dis*)

Following the suggestion obtained from computer simulations of the disordered phase (*LS-dis*) regarding the creation of micro twins, precise diffraction measurements of a single crystal of $[Fe(ptz)_6](BF_4)_2$ were carried out with a four-circle X-ray Xcalibur diffractometer using a Sapphire 3 CCD detector at 84 K in both the *LS-ord* (Fig. 9*a*) and *LS-dis* phases (Fig. 9*b*). Reconstruction of the reciprocal space was performed using *CryAlis* (Agilent, 2010). A detailed analysis of the reciprocal space showed that in the disordered phase, besides splitting of the reflection peaks of the high-temperature phase (*HS-R3*) additional weak satellite reflections appear (Fig. 9*b*). Surprisingly, these new peaks are not split. In contrast to *hkl* reflections, the main *00l* reflections are also not split. Splitting between the main peaks increases with increasing absolute value of the indices *h* (Fig. 9*c*) or *k* (Fig. 9*d*).

A detailed analysis of the diffraction peaks carried out for the disordered phase showed that the obtained patterns can be interpreted as the superposition of diffraction patterns of

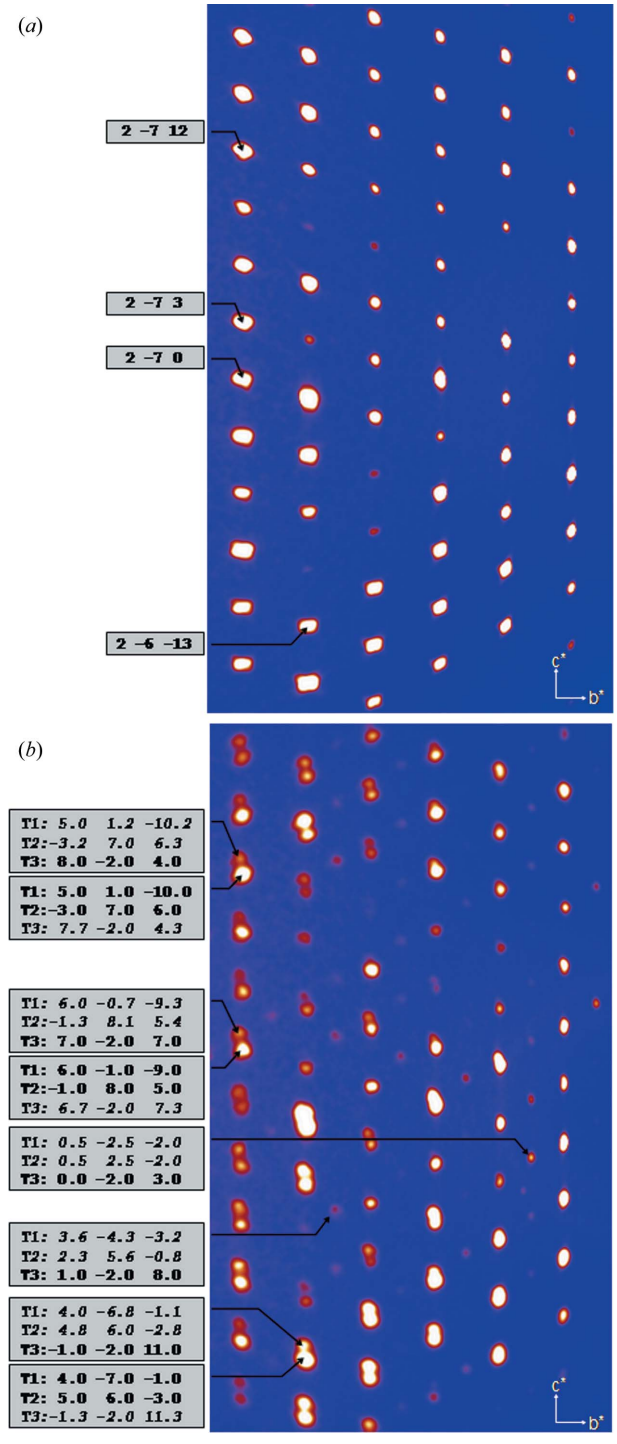

Figure 10
The (2*kl*) plane at 84 K for (*a*) the ordered LS phase (*LS-ord*) and (*b*) the disordered phase (*LS-dis*). In the ordered phase (*a*) the marked reflections can all be indexed with integer *hkl* values in the hexagonal phase. (*b*) Triclinic indices of split main reflections and new non-split reflections. The split reflections correspond to two slightly separated reflections from all three twins, while the non-split reflections correspond to just one of the three twins. This latter group lies at $k + \frac{1}{2}$ in the hexagonal reciprocal lattice.

three twins with lattices parameters a = 11.8799 (11), b = 10.7664 (4), c = 16.2919 (11) Å, α = 90.596 (4), β = 99.283 (7), γ = 89.642 (5)° and volume equal to 2056.4 (2) Å^3. To accommodate the pseudosymmetry an *I*-centred triclinic unit cell was chosen. Similar lattice parameters were proposed by Wiehl *et al.* from powder diffraction measurement and tensor analysis (Wiehl *et al.*, 1990). The analysis performed with *CrysAlis* software revealed that the main reflections are split because they belong to all three twin components (Fig. 10). The satellite reflections that exist only in the LS phase are not split because they only belong to one of the three twins. This has been explained in Fig. 10(*b*) owing to the new features of the *CrysAlis* program.

The mutual orientation of the rhombohedral and triclinic lattices is shown in Fig. 11. Three twins are shown which can be transformed from one to another by rotation around the twinning vector by 120°. The twinning vector makes an angle of 4.47° with the hexagonal c axis.

Comparison of the (*hk0*) layers between the *LS-ord* (Fig. 12*a*) and *LS-dis* (Fig. 12*b*) phases in the triclinic system shows that in the disordered phase two additional types of reflections appear: reflections with integer triclinic *hkl* indices that violate the I centring (*R* in the hexagonal system) and additional satellite reflections with indices $h + 1/2, k + 1/2, l$. Detailed analysis of the triclinic (*hk0*) plane at 84 K for the ordered LS phase (*LS-ord*) and the disordered phase (*LS-dis*) with marked peak indices in the triclinic system for three twin domains is shown in Figs. 12(*c*) and (*d*). In this description, all additional reflection types can be described as integer reflections that violate the triclinic I centring of one of the three twins.

For the optimal data reduction of the diffraction measurements obtained it is simplest to use a superlattice description with lattice parameters $(a + b)x(a - b)xc$ that is a = 16.1235 (12), b = 16.0450 (11), c = 16.3134 (12) Å, α = 83.583 (6), β = 96.870 (6), γ = 95.663 (6)°. In this superstructure integer Miller indices can be associated with all diffraction peaks and the split peak can be integrated as one Bragg peak (Fig. 12*e*).

This approach avoids the problem concerning independent integration of peak intensities for the three twin domains and also the problem connected with the separation and extraction of intensities from overlaying diffraction peaks. Whilst solving and refining the crystal structure it is necessary to treat the structure as a merohedral twin (Sheldrick, 2008).

The mutual orientation of the rhombohedral and the new triclinic lattice (superstructure) is shown in Fig. 13(*a*). Three twins are shown which can be transformed from one to another by 120° rotation as shown in Fig. 13(*a*). The reciprocal space model shown in Fig. 13(*b*) was obtained on the basis of calculations using triclinic superstructure orientation matrices determined using *CrysAlis* software for three twin components. The description as a superstructure illustrates how much easier it is for the three twin lattices to penetrate each other and why only some reflections are split. The presented model also explains why reflections only split into two maxima along the c^* direction. This is due to the very similar lattice parameters a, b, c and angles β and γ. Usually in a transition from a trigonal to a triclinic crystallographic system Bragg peaks split into three maxima, as observed in the case of the $[Fe(bbtr)_3](ClO_4)_2$ complex compound (Kusz, Bronisz *et al.*, 2011). In the present system under study an additional process occurs, *viz.* the creation of microdomains which leads to diffuse broadening of reflections. Owing to the fact that microdomains create lamella consisting of molecular layers parallel to the *ab* plane (in hexagonal description) reflections are diffused along the c^* direction. As can be seen it is a very unusual example of twinning for many reasons.

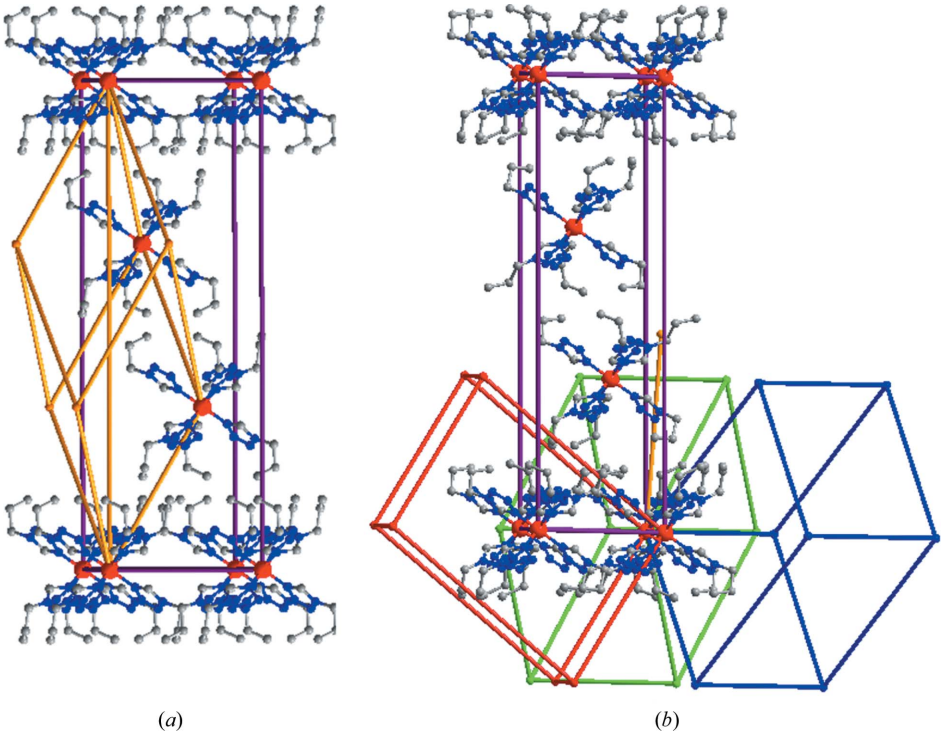

(*a*) (*b*)

Figure 11
Left: mutual orientation of the *R*-centred hexagonal and primitive rhombohedral lattices; right: hexagonal and triclinic lattices for the three twin domains. The rotation vector is 4.47° to the hexagonal c axis.

3.3.1. Determination of the LS disordered (*LS-dis*) structure. The structure of the disordered phase (*LS-dis*) at 84 K was solved using the data collection method described above. The structure was solved in the space group $P\bar{1}$ using the charge-flipping method with the *SuperFlip* program

(Palatinus & Chapuis, 2007; van Smaalen *et al.*, 2003) and the solution was refined using the *SHELXL*97 program (Sheldrick, 2008). The most important results of the superstructure refinement using the method described above are presented in Table 1. All non-H atoms were refined with anisotropic displacement parameters. The aromatic H atoms were treated as 'riding' on their parent C atoms with d(C—H) = 0.95 Å and assigned isotropic atomic displacement parameters equal to 1.2 times the value of the equivalent atomic displacement parameters of the parent C atom [U_{iso}(H) = 1.2U_{eq}(C)]. The methylene H atoms were constrained to an ideal geometry with d(C—H) = 0.99 or d(C—H) = 0.95 Å (for terminal methylene group) and U_{iso}(H) = 1.2U_{eq}(C). Methyl H atoms were constrained as riding atoms, fixed to the parent atoms with a distance of 0.98 Å and U_{iso}(H) = 1.5U_{eq}(C). The unit cell contains four molecules (Z = 4), where two of them were refined and the inversion centre generates the remaining two. A detailed analysis showed that the two refined molecules are identical within error limits and can be transformed into each other by the symmetry operator $(x+\frac{1}{2}, y+\frac{1}{2}, z)$, *i.e.* a C lattice centring. Based on this, the refinement of the structure was repeated using only one independent molecule in the non-standard space group $C\bar{1}$. The results obtained are presented in Table 1. As seen, the $R1$ agreement factor slightly increases

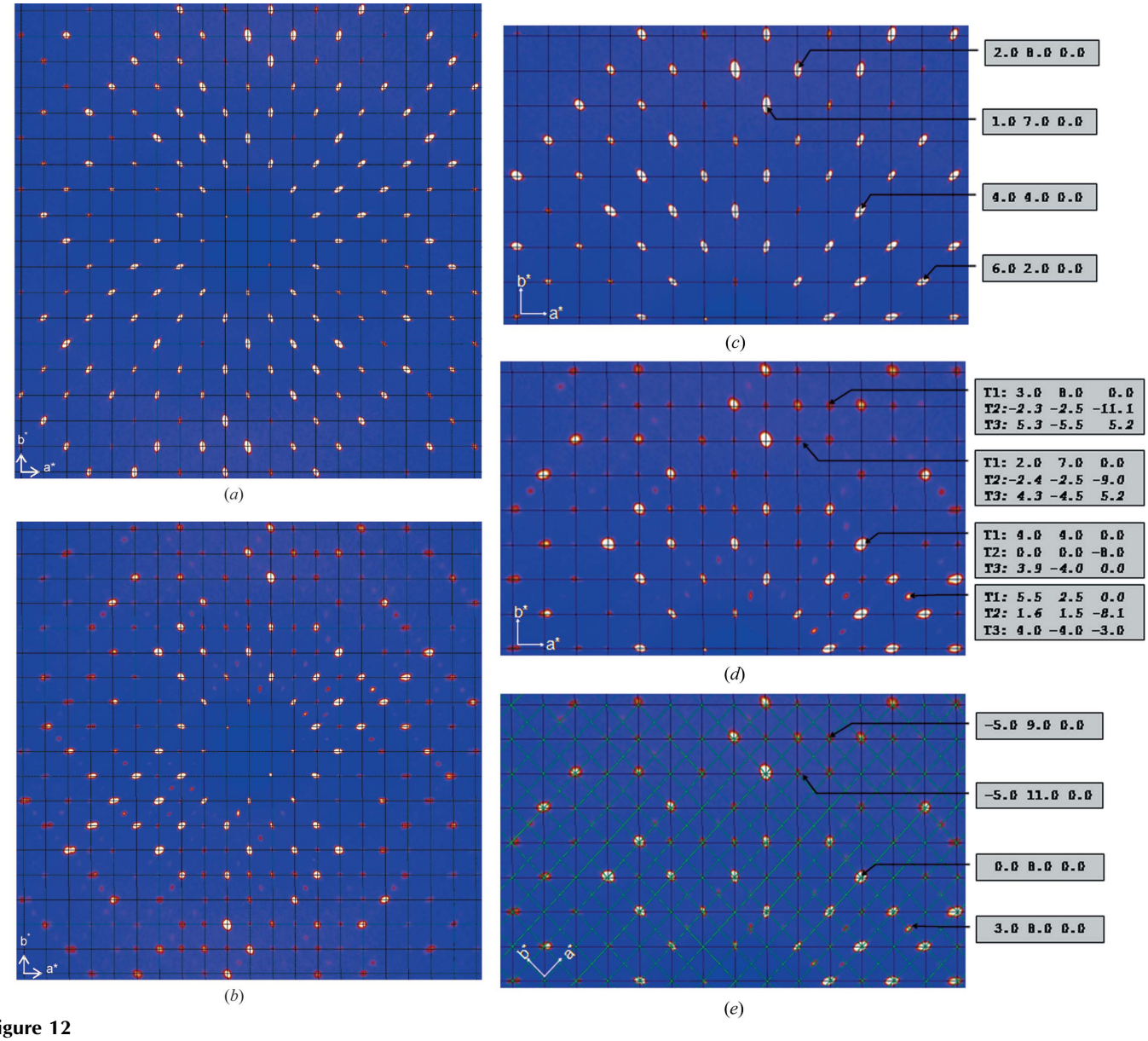

Figure 12
Triclinic (*hk*0) layer at 84 K in: (*a*) the LS supercooled phase (*LS-ord*); (*b*) the LS disordered phase (*LS-dis*); (*c*) the magnified triclinic (*hk*0) layer at 84 K in the ordered LS phase (*LS-ord*) and (*d*)–(*e*) the disordered phase (*LS-dis*). In the *LS-ord* phase (*c*) only integer reflections are observed. In the *LS-dis* phase (*d*) additional reflections appear that violate the *I*-centring of twin (I) or are at non-integer positions for twin (I). The latter can be indexed with integer *hkl* for one of the other two twin domains. (*e*) All reflections of the *LS-dis* phase can be indexed using a single domain triclinic superstructure.

Table 1
Details of data collection, refinement and structural parameters for $[Fe(ptz)_6](BF_4)_2$ measured at 84 K.

Columns one and two show the two models for the disordered LS phase, column four the ordered LS phase. Column three shows the corresponding values for the ordered LS phase for a refinement using the same unit cell and space group as the disordered phase. For all structures: $C_{24}H_{48}FeN_{24}\cdot 2BF_4$, M_r = 902.33

Compound reference	*LS-dis* ($P\bar{1}$)	*LS-dis* ($C\bar{1}$)	*LS-ord* ($C\bar{1}$)	*LS-ord* ($R\bar{3}$)
Crystal data				
Crystal system, space group	Triclinic, $P\bar{1}$	Triclinic, $C\bar{1}$	Triclinic, $C\bar{1}$	Rhombohedral, $R\bar{3}$
a, b, c (Å)	16.1235 (12), 16.0450 (11), 16.3134 (12)	16.1235 (12), 16.0450 (11), 16.3134 (12)	16.3473 (2), 16.3475 (2), 16.3475 (2)	10.7023 (2), 10.7023 (2), 32.0931 (15)
α, β, γ (°)	83.583 (6), 96.870 (6), 95.663 (6)	83.583 (6), 96.870 (6), 95.663 (6)	81.8150 (10), 98.1750 (10), 98.1800 (10)	90, 90, 120
V (Å^3)	4148.2 (5)	4148.2 (5)	4246.89 (9)	3183.44 (17)
Z	4	4	4	3
μ (mm^{-1})	0.45	0.45	0.44	0.44
Crystal size (mm)	0.61 × 0.53 × 0.14	0.61 × 0.53 × 0.14	0.61 × 0.53 × 0.14	0.61 × 0.53 × 0.14
Data collection				
Absorption correction	Multi-scan	Multi-scan	Multi-scan	Multi-scan
T_{min}, T_{max}	0.770, 0.939	0.771, 0.939	0.774, 0.941	0.774, 0.941
No. of measured, independent and observed [$I > 2\sigma(I)$] reflections	24 788, 12 420, 8851	24 788, 12 420, 8851	13 053, 6402, 3391	6536, 1105, 1099
R_{int}	0.024	0.024	0.009	0.011
Refinement				
$R[F^2 > 2\sigma(F^2)]$, $wR(F^2)$, S	0.070, 0.218, 1.03	0.074, 0.224, 1.03	0.032, 0.123, 1.15	0.025, 0.067, 0.97
No. of reflections	12 420	12 420	6402	1105
No. of parameters	771	534	538	91
$\Delta\rho_{max}$, $\Delta\rho_{min}$ (e Å$_{-3}$)	0.72, −0.90	0.59, −0.79	0.39, −0.35	0.24, −0.25
Twin fraction	0.292 (1), 0.329 (1)	0.294 (1), 0.329 (1)	0.0	0.0

Computer programs used: *CrysAlis CCD* (Oxford Diffraction Ltd, 2008*a*), *CrysAlis RED* (Oxford Diffraction, 2008*b*), *SHELXS*97, *SuperFlip*, *SHELXL*97 (Sheldrick, 2008).

(from 0.070 to 0.074) as the number of refined parameters drops drastically, however, the goodness-of-fit is the same. Fig. 14 shows the $[Fe(ptz)_6](BF_4)_2$ structure in the disordered phase. Selected bond lengths and bond angles are presented in Table 2.

These results show that the use of a superstructure as an approximate description of the disordered *LS-dis* phase is very useful and the use of the pseudosymmetry $C\bar{1}$ space group is required. In Fig. 12(*e*) the extinctions due to C centring are not observed because in these positions peaks from other twin components appear. Reflections in these points of reciprocal space are not split because they only belong to one twin component.

3.3.2. Comparison of the structures of *LS-ord* and *LS-dis*. In order to compare the low-spin structure of the disordered (*LS-dis*) phase with that of the ordered (*LS-ord*) phase at the same temperature (84 K), an additional measurement on the same crystal after rapid cooling was performed. An accurate crystal structure analysis was performed in the same pseudosymmetric space group $C\bar{1}$. The results are shown in Table 1. For comparison, the structure was also refined in the rhombohedral space group $R\bar{3}$ (Table 1). The results for both symmetries are very similar. Crucial bond lengths, bond angles and torsion angles are presented in Table 2. The differences between these values of the two phases are also presented in this table. The *LS-dis* phase molecule $[Fe(ptz)_6]$ is non-centrosymmetric (the Fe ion is not placed at the inversion centre), in contrast to the *LS-ord* phase. Structurally ligands 5 and 6 (see Figs. 14 and 15) of the *LS-dis* phase are only slightly different from ligands 5 and 6 of the *LS-ord* phase, but ligands 2 and 3 are drastically different. Differences in the N204—C202—C203—C204 torsion angle are 132.9° and for the N304—C302—C303—C304 torsion angle are 115.3°. Such differences arise from the change of geometry of those two ligands. The difference between the two remaining ligands is not crucial. Also the anions are rotated with respect to each other in the two phases.

Straightening of the propyl groups gives rise to the formation of new short contacts between adjacent molecular layers (Fig. 16). Distances between layers (Fig. 16) in the disordered phase decreased significantly from 10.699 Å in *LS-ord* to 10.399 Å in *LS-dis*.

This difference in ligand geometry is consistent with Raman (Moussa *et al.*, 2005) and NIS (Böttger *et al.*, 2006) measurements. Also DFT calculations (Böttger *et al.*, 2006) showed the existence of characteristic markers for the disordered phases of *LS-dis* and *LIESST-HS-dis* on Raman spectra corresponding to the propyl group vibrations. Such changes of the ligands lead to alterations of interlayer distances.

Similar ligand geometry and torsion angles occur in the $[Fe(ptz)_6](PF_6)_2$ complex compound in the high-spin phase (Jeftic *et al.*, 1997). This compound crystallizes in the space group $P\bar{1}$ with one molecule per unit cell (Z = 1). The molecules also form trigonal layers but their packing is completely

different from that in $[Fe(ptz)_6](BF_4)_2$. Adjacent layers are not created by the *R*-centring vector running along the longer diagonal of the hexagonal unit cell but by the vector running along the diagonal of the face of the pseudohexagonal unit cell. Layers are also shifted with respect to each other which is the basis for our computer simulations of the disordered phase of $[Fe(ptz)_6](BF_4)_2$. Unfortunately, the structure of $[Fe(ptz)_6](PF_6)_2$ was determined only in the high-spin state and it is not known whether the spin transition leads to a disordered structure (Jeftic *et al.*, 1997). However, it can be assumed that the low-spin phase is probably ordered because the spin transition in this compound does not reveal a hysteresis.

At 293 and 130 K the two propyl groups of the $[Fe(ptz)_6](PF_6)_2$ complex compound are also straightened and in opposite positions to each other in the centrosymmetric complex molecules. In the case of $[Fe(ptz)_6](BF_4)_2$ under study in the *LS-dis* phase only one propyl group is straightened and the corresponding Fe—N bond length is slightly longer.

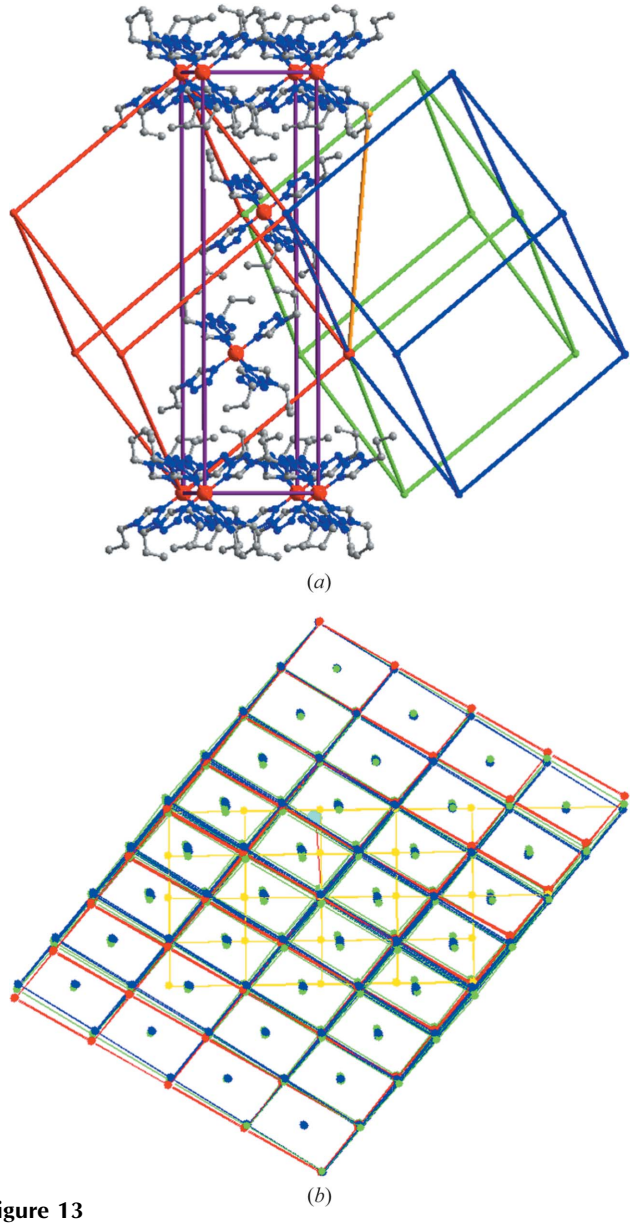

Figure 13
(*a*) The mutual orientation of hexagonal and triclinic superstructure lattices. (*b*) Reciprocal space model obtained on the basis of calculations performed using triclinic superstructure orientation matrices determined by means of *CrysAlis* software for three twin components. The hexagonal reciprocal lattice is marked in yellow. This calculation shows how single peak reflections and split reflections arise. The split reflections consist of two reflections that are very close to each other and completely overlap in the experiment and a third reflection further away.

4. Conclusions

The appearance of a new high-spin phase, at low temperatures, after crystal irradiation with laser light (LIESST) is a phenomenon often observed in SCO complex compounds. $[Fe(ptz)_6](BF_4)_2$ is unique because it undergoes a phase transition to the disordered phase under slow cooling but preserves the structure on rapid cooling. Disorder in anions and solvents can have a drastic influence on the spin transition scenario, when hydrogen bonds are present. The best example of such a situation is the complex $[Fe(dpp)_2(NCS)_2]\cdot py$ (Kusz, Zubko *et al.*, 2011). Such effects are not observed in the present complex compound because BF_4 anions are ordered and there is a lack of hydrogen bonds.

So far no one has managed to explain this unusual phenomenon. Only after the computer simulations shed new light on this rare effect were we able to solve the structure of this disordered phase. The phase transition to the disordered phase in the $[Fe(ptz)_6](BF_4)_2$ compound proceeds in three steps.

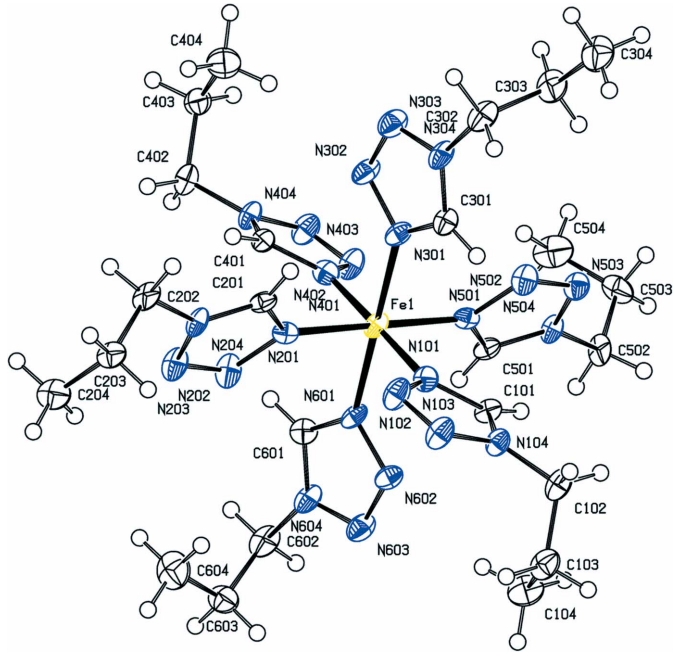

Figure 14
The structure of molecules for the *LS-dis* phase solved at 84 K. Anisotropic displacement parameters are drawn atthe 50% probability level.

Table 2
Bond lengths and bond angles of Fe-N_i and torsion angles for *LS-ord* and *LS-dis* phases for $[Fe(ptz)_6](BF_4)_2$ measured at 84 K.

$\Delta(dis - ord)$ is the difference between these values for the two phases.

	LS-ord	*LS-dis*	$\Delta(dis - ord)$
Bond lengths (Å)			
Fe1—N101	1.9964 (17)	1.9833 (53)	−0.0131 (70)
Fe1—N201	1.9940 (17)	1.9866 (45)	−0.0074 (62)
Fe1—N301	1.9899 (17)	2.0217 (53)	0.0318 (70)
Fe1—N401	1.9862 (17)	1.9861 (56)	−0.0001 (73)
Fe1—N501	1.9862 (17)	1.9867 (56)	0.0005 (73)
Fe1—N601	1.9926 (17)	2.0105 (51)	0.0179 (68)
Bond angles (°)			
N101—Fe1—N201	90.52 (7)	90.90 (19)	0.38 (26)
N101—Fe1—N301	89.50 (7)	89.9 (2)	0.40 (9)
N101—Fe1—N401	179.86 (9)	179.14 (11)	−0.72 (20)
N101—Fe1—N501	89.47 (7)	89.4 (2)	−0.07 (9)
N101—Fe1—N601	90.39 (7)	89.8 (2)	−0.59 (9)
N201—Fe1—N301	89.36 (7)	90.31 (19)	0.95 (26)
N401—Fe1—N201	89.61 (7)	88.98 (19)	−0.63 (26)
N201—Fe1—N501	179.89 (9)	179.21 (11)	−0.68 (20)
N201—Fe1—N601	90.58 (7)	89.62 (19)	−0.96 (26)
N401—Fe1—N301	90.55 (7)	91.0 (2)	0.45 (9)
N501—Fe1—N301	90.53 (7)	90.4 (2)	−0.13 (9)
N401—Fe1—N501	90.40 (7)	90.8 (2)	0.40 (9)
N401—Fe1—N601	89.55 (7)	89.4 (2)	−0.15 (9)
N501—Fe1—N601	89.53 (7)	89.64 (19)	0.11 (26)
N601—Fe1—N301	179.88 (8)	179.65 (11)	−0.23 (19)
Torsion angle (°)			
N104—C102—C103—C104	58.6 (2)	57.4 (6)	−1.2 (8)
N204—C202—C203—C204	58.8 (2)	−74.1 (6)	−132.9 (8)
N304—C302—C303—C304	−58.1 (2)	−173.4 (4)	−115.3 (6)
N404—C402—C403—C404	−58.6 (3)	−56.6 (5)	2.0 (8)
N504—C502—C503—C504	−58.6 (2)	−56.8 (6)	1.8 (8)
N604—C602—C603—C604	59.1 (2)	58.5 (6)	−0.6 (8)
N103—N104—C102—C103	60.8 (3)	76.7 (6)	15.9 (9)
N203—N204—C202—C203	60.3 (2)	59.6 (7)	−0.7 (9)
N303—N304—C302—C304	−61.2 (3)	−89.7 (6)	−28.5 (9)
N403—N404—C402—C403	−60.7 (3)	−74.5 (7)	−13.8(10)
N503—N504—C502—C503	−61.3 (2)	−67.7 (7)	−6.4 (9)
N603—N604—C602—C603	60.5 (3)	62.7 (6)	2.2 (9)
C101—N104—C102—C103	−125.6 (2)	−100.8 (7)	24.8 (9)
C201—N204—C202—C203	−125.2 (2)	−131.9 (7)	−6.7 (9)
C301—N304—C302—C304	125.0 (2)	87.6 (8)	−37.4(10)
C401—N404—C402—C403	124.8 (2)	107.5 (7)	−17.3 (9)
C501—N504—C502—C503	125.5 (2)	116.2 (7)	−9.3 (9)
C601—N604—C602—C603	−125.6 (2)	−116.5 (7)	9.1 (9)

(i) By lowering the temperature the spin transition occurs to the LS state.

(ii) This immediately involves drastic changes in the lattice parameters and an increase in the distance between the electrically neutral molecular layers which form the crystal structure.

(iii) Afterwards (in this LS state) a gradual lowering of the symmetry from $R\bar{3}$ to $P\bar{1}$ occurs (probably due to weakening of the van der Waals forces between adjacent layers) leading to a disorder phase.

What is interesting is that during the heating of the sample the peak broadening and splitting return to the previous form and this process is reversible. However, when the sample is rapidly cooled below the spin transition temperature (135 K) a significant change in the lattice parameters is also observed, but the symmetry is retained and all the Bragg reflections remain sharp.

Based on analysis of the lattice parameters (described in earlier work), we concluded that the transition to the disordered phase is related to the anomalous expansion associated with the spin transition. This leads to a significant weakening of the van der Waals interactions between layers in the temperature range from 135 to 100 K. As a consequence, electrically neutral layers shift perpendicularly to the hexagonal *c* axis. As shown in this paper, the rate of the phase transition associated with the formation of the disorder is dependent on the temperature. Owing to the disappearance of this process at 90 K, we can obtain the low-temperature ordered phase (LS-ord) by rapid cooling. This hypothesis should be further verified by calculating the temperature change of the van der Waals interactions between the layers.

Until now, it has not been possible to understand the low-temperature disordered phase. Diffuse X-ray scattering gives important information about the short-range order which exists after this phase transition. As shown by computer simulations with increasing holding time at constant temperature the amount of layers that take part in the twinning increases and micro twins are being created as seen by the growth of the second peak and the increase of the FWHM of the first peak.

The computer simulations performed for the *LIESST-HS-dis* phase, which exists after irradiation the *LS-dis* phase below 50 K, showed the existence of micro twins similar to those in *LS-dis*.

Comparing the structures of the *LS-ord* and *LS-dis* phases, solved for the same temperature of 84 K, significant differences are observed in ligand positions (especially for propyl groups).

Structural studies of the disordered phase revealed that the main difference between the molecules in the *LS-ord* and *LS-dis* phases is the shape of the *n*-propyl (C1—C2–C3) chains for

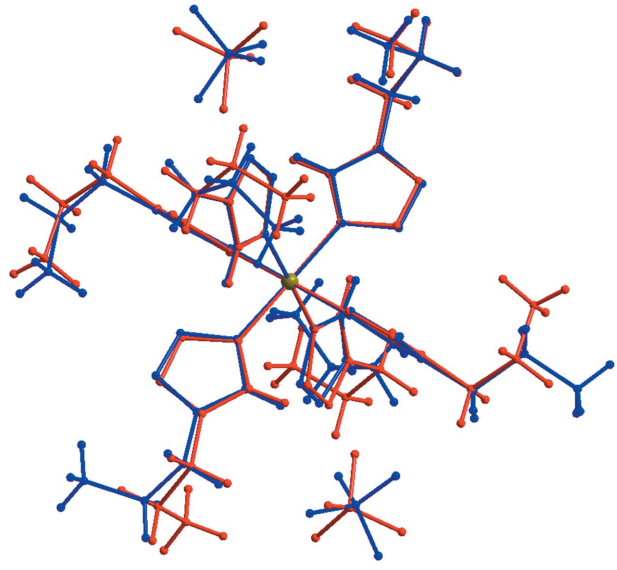

Figure 15
Structural comparison of two molecules for phases *LS-ord* and *LS-dis* at 84 K.

two of the six ligands. This is confirmed by Raman (Moussa *et al.*, 2005) and synchrotron NIS (Böttger *et al.*, 2006) measurements, and also by DFT calculations (Böttger *et al.*, 2006), which showed significant differences between the ordered and disordered phases. Raman spectra revealed characteristic 'peak markers' for the disordered phase (Moussa *et al.*, 2005). Results from DFT calculations led to the conclusion that such peaks originate from vibrations of the *n*-propyl bending modes. Coupling of the Fe—N stretching vibrations with those of the terminal *n*-propyl groups is also a sensitive marker in the NIS spectra for crystallographic order–disorder transitions (Böttger *et al.*, 2006).

Summarizing we may say that in the spin-crossover compound $[Fe(ptz)_6](BF_4)_2$ the structural phase transition at ambient pressures is induced by the spin-state transition. This is supported by the fact that the isostructural $[Zn(ptz)_6](BF_4)_2$ complex compound does not undergo any structural phase transition. The other possibility is that the structural phase transition causes a spin-state transition. An example of such behaviour is the complex compound $[Fe(bbtr)_3](ClO_4)_2$. In this compound a structural phase transition (from trigonal $P\bar{3}$ to triclinic $P\bar{1}$) is observed a few degrees above the spin-state transition (Kusz, Bronisz *et al.*, 2011). The same structural phase transition is observed in the isostructural $[Zn(bbtr)_3](ClO_4)_2$ compound. For the isostructural $[Zn(bbtr)_3](BF_4)_2$ complex compound the phase transition is not observed and therefore the complex $[Fe(bbtr)_3](BF_4)_2$ remains in a high spin-state over the whole temperature range. This means that in the $[Fe(bbtr)_3](ClO_4)_2$ complex compound the structural phase transition provides the conditions for the subsequent spin transition to occur (Kusz, Bronisz *et al.*, 2011).

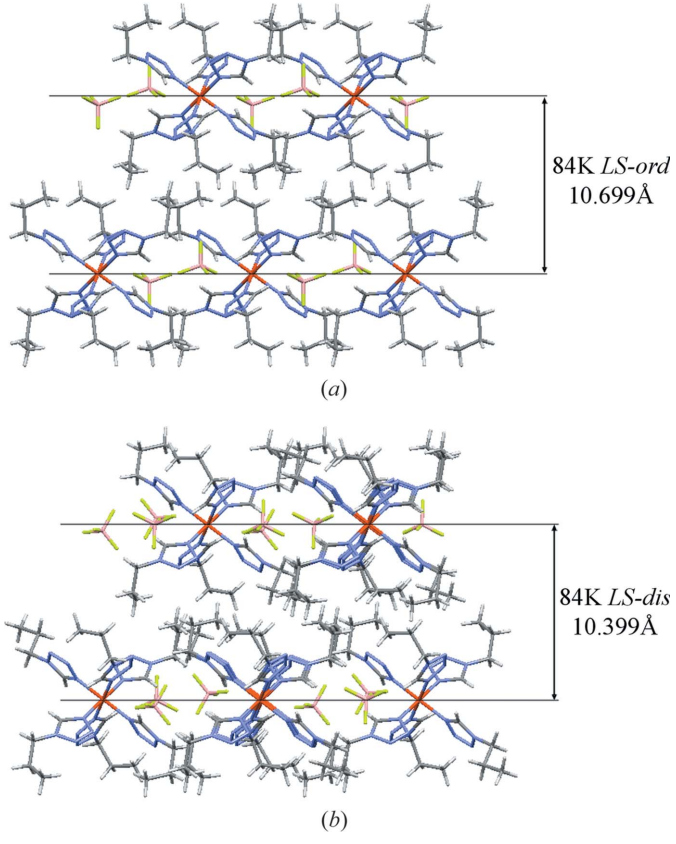

Figure 16
Comparison of two molecular layers for phases (*a*) *LS-ord* and (*b*) *LS-dis* at 84 K. The interlayer distances have been marked for clarity.

The work was partially supported by the Polish National Science Centre Grant No. DEC-2011/01/B/ST5/06311. We also thank the Deutsche Forschungsgemeinschaft (DFG) for financial support (Priority Program 1137 'Molecular Magnetism').

References

Agilent (2010). *CrysAlis PRO*, Version 1.171.35. Agilent Technologies, Yarnton, Oxfordshire, England.
Böttger, L. H., Chumakov, A. I., Grunert, C. M., Gütlich, P., Kusz, J., Paulsen, H., Ponkratz, U., Rusanov, V., Trautwein, A. X. & Wolny, J. A. (2006). *Chem. Phys. Lett.* **429**, 189–193.
Chong, C., Mishra, H., Boukheddaden, K., Denise, S., Bouchez, G., Collet, E., Ameline, J., Naik, A. D., Garcia, Y. & Varret, F. (2010). *J. Phys. Chem. B*, **114**, 1975–1984.
Decurtins, S., Gütlich, P., Hasselbach, K. M., Hauser, A. & Spiering, H. (1985). *Inorg. Chem.* **24**, 2174–2178.
Decurtins, S., Gütlich, P., Köhler, C. P., Spiering, H. & Hauser, A. (1984). *Chem. Phys. Lett.* **105**, 1–4.
Franke, P. L. (1982). Thesis. Rijks University, Leiden.
Franke, P. L., Haasnoot, J. G. & Zuur, A. P. (1982). *Inorg. Chim. Acta*, **59**, 5–9.
Gałdecka, E. (2002). *J. Appl. Cryst.* **35**, 641–643.
Goujon, A., Gillon, B., Debede, A., Cousson, A., Gukasov, A., Jeftic, J., McIntyre, G. J. & Varet, F. (2006). *Phys. Rev. B*, **73**, 104413.
Goujon, A., Varret, F., Boukheddaden, K., Chong, C., Jeftic, J., Garcia, Y., Naik, A. D., Ameline, J. C. & Collet, E. (2008). *Inorg. Chim. Acta*, **361**, 4055–4064.
Gütlich, P. & Goodwin, H. A. (2004). *Spin Crossover in Transition Metal Compounds*, in *Topics in Current Chemistry*, Vol. 233, pp. 234–235. New York: Springer.
Gütlich, P., Hauser, A. & Spiering, H. (1994). *Angew. Chem. Int. Ed. Engl.* **33**, 2024–2054.
Hauser, A., Gütlich, P. & Spiering, H. (1986). *Inorg. Chem.* **25**, 4245–4248.
Jeftic, J., Gillon, B., Goujon, A., Nau, Q., Gukasov, A., Codjovi, E. & Varret, F. (2003). *Polyhedron*, **22**, 2155–2160.
Jeftic, J. & Hauser, A. (1997). *J. Phys. Chem. B*, **101**, 10262–10270.
Jeftic, J., Hinek, R., Capelli, S. C. & Hauser, A. (1997). *Inorg. Chem.* **36**, 3080–3087.
Jeftic, J., Romstedt, H. & Hauser, A. (1996). *J. Phys. Chem. Solids*, **57**, 1743–1750.
Jung, J., Spiering, H., Yu, Z. & Gütlich, P. (1995). *Hyperfine Interact.* **95**, 107–128.
Kusz, J., Böhm, H. & Gütlich, P. (2001). *Proceedings of XVIII Conference on Applied Crystallography*, edited by H. Morawiec & D. Stróż, pp. 104–107. Singapore: World Scientific.
Kusz, J., Bronisz, R., Zubko, M. & Bednarek, G. (2011). *Chem. Eur. J.* **17**, 6807–6820.
Kusz, J., Gütlich, P. & Spiering, H. (2004). *Top. Curr. Chem.* **234**, 129–153.
Kusz, J., Spiering, H. & Gütlich, P. (2000). *J. Appl. Cryst.* **33**, 201–205.
Kusz, J., Spiering, H. & Gütlich, P. (2001). *J. Appl. Cryst.* **34**, 229–238.
Kusz, J., Spiering, H. & Gütlich, P. (2004). *J. Appl. Cryst.* **37**, 589–595.
Kusz, J., Spiering, H., Hinek, R. & Gütlich, P. (1996). *Workshop on Aperiodic Structures*, p. 185. Krakow, Poland.
Kusz, J., Zubko, M., Fitch, A. & Gütlich, P. (2011). *Z. Kristallogr.* **226**, 576–584.

Lakhloufi, S., Guionneau, P., Lemée-Cailleau, M. H., Rosa, P. & Létard, J. F. (2010). *Phys. Rev. B*, **82**, 132104.
Moritomo, Y., Kato, K., Nakamoto, A., Kojima, N., Nishibori, E., Takata, M. & Sakata, M. (2002*a*). *J. Phys. Soc. Jpn*, **71**, 1015–1018.
Moritomo, Y., Kato, K., Nakamoto, A., Kojima, N., Nishibori, E., Takata, M. & Sakata, M. (2002*b*). *J. Phys. Soc. Jpn*, **71**, 2609–2612.
Moussa, N. O., Molnar, G., Ducros, X., Zwick, A., Tayagaki, T., Tanaka, K. & Bousseksou, A. (2005). *Chem. Phys. Lett.* **402**, 503–509.
Müller, E. W., Ensling, J., Spiering, H. & Gütlich, P. (1983). *Inorg. Chem.* **22**, 2074–2078.
Neder, R. B. & Proffen, Th. (2008). *Diffuse Scattering and Defect Structure Simulation.* Oxford University Press.
Oxford Diffraction (2008*a*). *CrysAlis CCD*. Oxford Diffraction Ltd, Abingdon, England.
Oxford Diffraction (2008*b*). *CrysAlis RED*. Oxford Diffraction Ltd, Abingdon, England.
Ozarowski, A. & McGarvey, B. R. (1989). *Inorg. Chem.* **28**, 2262–2266.
Palatinus, L. & Chapuis, G. (2007). *J. Appl. Cryst.* **40**, 786–790.
Proffen, Th. & Neder, R. B. (1997). *J. Appl. Cryst.* **30**, 171–175.
Sheldrick, G. M. (2008). *Acta Cryst.* A**64**, 112–122.
Stoe (1995). *STADI4 Software Manual.* Stoe and Cie, Darmstadt, Germany.
van Smaalen, S., Palatinus, L. & Schneider, M. (2003). *Acta Cryst.* A**59**, 459–469.
Wiehl, L. (1993). *Acta Cryst.* B**49**, 289–303.
Wiehl, L., Spiering, H., Gütlich, P. & Knorr, K. (1990). *J. Appl. Cryst.* **23**, 151–160.
Zubko, M., Zajdel, P. & Kusz, J. (2010). *Solid State Phenom.* **163**, 46–50.